THE JOURNAL OF PHYSICAL CHEMISTRY A

Article

Organic Enrichment at Aqueous Interfaces: Cooperative Adsorption of Glucuronic Acid to DPPC Monolayers Studied with Vibrational Sum Frequency Generation

Katie A. Link, Gabrielle N. Spurzem, Aashish Tuladhar, Zizwe Chase, Zheming Wang, Hongfei Wang, and Robert Allan Walker

J. Phys. Chem. A, **Just Accepted Manuscript** • Publication Date (Web): 04 Jun 2019

Organic Enrichment at Aqueous Interfaces: Cooperative Adsorption of Glucuronic Acid to DPPC Monolayers Studied with Vibrational Sum Frequency Generation

Katie A. Link,[a] Gabrielle N. Spurzem,[a] Aashish Tuladhar,[c] Zizwe Chase,[d] Zheming Wang,[c] Hongfei Wang,[e] and Robert A. Walker[a,b,]*

[a]Department of Chemistry and Biochemistry, Montana State University, Bozeman, MT, 59717, USA

[b]Montana Materials Science Program, Montana State University, Bozeman, MT, 59717, USA

[c]Physical Sciences Division, Physical and Computational Sciences Directorate, Pacific Northwest National Laboratory, Richland, Washington, 99352, USA

[d]Department of Physics and Astronomy, Howard University, Washington, D.C., 20059, USA

[e]Department of Chemistry and Shanghai Key Laboratory of Molecular Catalysis and Innovative Materials, Fudan University, Shanghai, 200433, China

Corresponding Author: rawalker@montana.edu

ABSTRACT

Surface tension, surface-specific vibrational spectroscopy and differential scanning calorimetry measurements were all used to test cooperative adsorption of glucuronic acid (GU) to DPPC monolayers adsorbed to the aqueous/vapor interface. Experiments were performed using GU solutions prepared in Millipore water and in carbonate/bicarbonate solutions buffered to a pH of 9.0. The effects of GU on DPPC monolayer structure and organization were carried out with tightly packed monolayers (40 Å^2/DPPC) and monolayers in their liquid condensed phase (55 Å^2/molecule). Surface tension data show that GU concentrations of 50 mM lead to expanded DPPC monolayers with diminished surface tensions (or higher surface pressures) at a given DPPC coverage relative to monolayers on pure water. With unbuffered solutions, GU induces significant ordering within liquid condensed monolayers although the effects of GU on tightly packed DPPC monolayers are less pronounced. GU also induces a second, higher melting temperature in DPPC vesicles implying that GU (at sufficiently high concentrations) strengthens lipid-lipid cohesion, possibly by replacing water solvating the DPPC headgroups. Together, these observations all support a cooperative adsorption mechanism. In buffer solutions, the effects of dissolved GU on DPPC structure and organization are muted. Only at sufficiently high GU concentrations (when the solution's buffering capacity has been exceeded) do the data again show evidence of cooperative adsorption. These findings place limits on cooperative

adsorption's ability to enrich interfacial organic content in alkaline environmental systems such as oceans.

1. INTRODUCTION

Correlating molecular behavior to global phenomena is a tenuous exercise, but sea spray aerosols (SSAs) can provide such a link. Globally, SSAs serve as cloud condensation nuclei[1, 2] and ice condensation nuclei,[3] both of which affect cloud lifetime and radiative properties.[3, 4] Cloud formation and cloud dynamics are critical variables in models used to determine global albedo and the impact of solar energy retention on global climate change. The efficacy of SSA to form clouds is significantly enhanced by SSA organic content,[5, 6] and recent field studies have reported surprisingly high organic content in freshly formed SSAs prompting the question of how this organic matter was incorporated into the aerosol droplets.[2] SSAs can be produced in several different ways. One source of SSA production occurs when bubbles burst at the ocean surface creating film drops (typically < 1 μm in diameter) from the bubble remnants. The void at the surface left by the bubble bursting results in a jet that produces larger bubbles (2-20 μm in diameter). Aerosols can also be produced from larger drops that are formed when spume is pulled off of waves, usually due to high winds. Large splash drops can contribute to SSAs, but these are typically too large to remain suspended and mostly propagate smaller aerosol formation through the other mechanisms.[7, 8]

SSAs are complex and chemically heterogeneous systems. Primary aerosol emissions at the ocean surface are responsible for ~50% of all aerosol mass,[9] and SSA organic content is often enriched in comparison to the dissolved oceanic organic content.

Saccharide concentration at the sea surface microlayer (SSML) is 1-10x the concentration of salt (0.4 - 0.5 mM), and the concentration ratio of saccharide to salt is even greater in SSA with an enrichment of more than 10^3 having been observed in fine SSA particles.[8] SSAs can contain a collection of additional organic and biological molecules acquired from the sea-surface microlayer. These organic and biological molecules include protein fragments, phytoplankton, lipids, among other species. SSA organic content is important given the link between SSAs and cloud nucleation.[3] These empirical observations, however, cannot account for the fact that SSAs often show organic enrichment – up to 77% by mass[10] – beyond what one would predict based simply on insoluble surfactant films adsorbed to the water-air interface when the aerosols form.

One proposed mechanism developed to account for organic enrichment in SSAs is a cooperative adsorption model.[11] Cooperative adsorption describes interactions between an insoluble Langmuir film adsorbed to the aqueous/vapor interface and soluble organics that would not normally be enriched at the surface. This cooperative interaction arises from noncovalent interactions and drives soluble organics to the surface to associate with the headgroups of insoluble monomers comprising the Langmuir film. A previous study of saccharide adsorption to a DPPC interface showed Langmuir adsorption behavior with a $C_{1/2,gluc,2} = 1.25 \pm 0.45$ mM glucosamine.[11] This work and other reports proposed that cooperative adsorption arose from Coulombic interactions between zwitterionic lipid headgroups and positively charged monosaccharides.[11, 12] These studies did not consider how *negatively* charged species might interact with the zwitterionic lipid films in chemically complex systems (such as buffered solutions and/or high ionic strengths). Experimental findings cited above have recently been integrated into the OCEANFILMS modeling program designed to improve simulations of primary aerosol mass.[13] Another recent climate model on marine primary organic aerosols found that reducing surface tension (i.e. by increasing interfacial organic content) resulted in more marine primary organic aerosols being activated to form cloud droplets leading to smaller cloud droplet effective radii and a stronger indirect radiative effect.[14]

Work described in this manuscript expands this examination of cooperative adsorption in model environmental systems. Specifically, a combination of vibrational sum frequency generation (VSFG) experiments, differential scanning calorimetry measurements and Langmuir surface pressure isotherms are used to test the ability of lipid films adsorbed to aqueous/vapor interfaces to draw anionic soluble saccharides to the aqueous/vapor interface. The lipid films consist of dipalmitoylphosphatidylcholine (DPPC) at different surface coverages on solutions containing the monosaccharide glucuronic acid (GU). The GU bulk concentration is varied between 1 and 100 mM in aqueous solutions having different ionic strengths and pH. DPPC is a zwitterionic phosphocholine molecule that was chosen, in part, because of its prevalence in biological membranes and widespread use as a surrogate in studies that examine lipid membrane structure and dynamics.[15-17] Glucuronic acid is the monomer unit of alginate and has a pKa of 3.20.[18] In ambient Millipore water (pH of 5.8) and in more alkaline solutions such as blood plasma (pH 7.4) and the ocean (8.1), glucuronic acid is deprotonated.[15-17] GU is not surface active as evidenced by both surface tension and spectroscopic data. (Vide infra.)

Results reported in this work show that negatively charged glucuronic acid can cause a moderately packed DPPC monolayer to become more organized and that this organization depends on GU concentration in the subphase. This reorganization induced by glucuronic acid is minimized when the DPPC monolayer is already tightly packed into a two-dimensional solid or when other aqueous ions compete with glucuronic acid for access to the zwitterionic DPPC headgroups. Most studies that examine solute ion effects on lipid monolayer organization have focused on divalent cations.[19-23] For example, in cation/DPPC systems the negatively charged phosphate group on the lipid head interacts strongly with the cation, especially if the cation is divalent such as Ca^{2+}, Mg^{2+}, or Zn^{2+}. The result of this interaction is monolayer condensation. DPPC, however, also has a positively charged tertiary amine. Interactions between solution phase anions and DPPC's positive but shielded charge are not often thought to be responsible for monolayer condensation. Nevertheless, the DPPC-GU systems studied in this work show strong evidence of anionic solutes interacting strongly with DPPC headgroups provided that the solution does not contain other charged species that will compete with the GU. Organic enrichment through this cooperative adsorption mechanism has yet to be addressed in models describing SSA formation.[24]

2. EXPERIMENTAL

2.1 Materials

1,2-dipalmitoyl-*sn-glycero*-3-phosphocholine (DPPC, powder, >99%) was purchased from Avanti Polar Lipids Inc. (Alabaster, Alabama). D-Glucuronic acid (GU, powder, ≥98%), sodium carbonate monobasic (powder, ≥99%), sodium carbonate dibasic (powder, ≥98%), and sodium hydroxide (pellets, ≥98%) were purchased from Sigma-Aldrich (St. Louis, MO). HPLC grade chloroform (99.9%) was purchased from Fisher Scientific. All chemicals were used without further purification. Millipore water (resistivity of 18.2 MΩ) was used for all aqueous sample preparation.

2.2 Preparation of Samples

Lipid stock solutions (0.7 mg/mL) were prepared in chloroform and sonicated for 20 minutes. Buffer solutions of pH 9.0 (100 mM) were made with sodium carbonate and sodium bicarbonate. Glucuronic acid (pKa 3.20) was added to buffer solutions before adjusting the pH of the solution to 9.0 with sodium hydroxide.

For VSFG experiments, aqueous samples were prepared in either a Teflon Petri dish or a Pyrex borosilicate Petri dish bottom. Teflon Petri dishes were cleaned with Liquinox (Alconox Inc.) and then rinsed with Millipore water before being treated with UV/ozone (Novascan PSD Pro Series Digital UV Ozone System). Borosilicate Petri dishes were acid washed (50/50 vol. nitric/sulfuric) and then rinsed multiple times with Millipore water before use. The DPPC-containing spreading solvent was deposited on the surface of the aqueous solution with a Hamilton glass microsyringe.

2.3. Vibrational Sum Frequency Generation

Vibrational sum frequency generation (VSFG) is a second order nonlinear spectroscopy technique that only probes molecular vibrations that are non-centrosymmetric. This capability allows study of molecules at surfaces without contributions from the bulk phase. To produce VSFG signal, two incident laser sources—a fixed 800 nm visible laser and a tunable IR source are combined spatially and temporally at a surface. If the IR source is resonant with a vibrational mode of surface species, the sum frequency signal becomes resonantly enhanced.

The sum frequency intensity, $I(\omega)$, (Equation 1a) is proportional to the square of the second-order nonlinear susceptibility $\chi^{(2)}$. The effective second-order nonlinear susceptibility is made up of a non-resonant part, $\chi^{(2)}_{NR,eff}$ and a resonantly enhanced term, , $\chi^{(2)}_{q,eff}$, that depends on the resonant frequency, ω_q, and the damping constant of the qth vibrational mode, Γ_q, (Equation 1b).[25] Recent studies have shown that at charged aqueous interfaces, the potential of the interface, $\Phi(0)$ can lead to mixing of the second and third order nonlinear susceptibilities, $\chi^{(3)}$;[26, 27] this mixing can also affect SF intensities and lineshapes, sometimes in non-intuitive ways (Equation 1c).

$$I(\omega) \propto |\chi^{(2)}_{eff}|^2 \quad (1a)$$

$$|\chi^{(2)}_{eff}|^2 = \left|\chi^{(2)}_{NR,eff} + \sum \frac{\chi^{(2)}_{q,eff}}{\omega_{IR} - \omega_q + i\Gamma_q}\right|^2 \quad (1b)$$

$$I(\omega) \propto \left|\chi^{(2)}_{NR} + \sum \frac{\chi^{(2)}_{q,eff}}{\omega_{IR} - \omega_q + i\Gamma_q} + (\chi^{(3)}_1 + i\chi^{(3)}_2)\Phi(0)\right|^2 \quad (1c)$$

Wen *et. al.* first developed a phase sensitive VSFG description that enabled them to investigate the effects of a charged interface on the electric double layer (EDL).[28] The mathematical treatise for $\chi^{(3)}$ effects on SFG and SHG (Second Harmonic Generation) arising from an EDL formed by a charged interface was furthered developed by Gonella *et. al.*[29] Shortly after, Wen *et. al.* deduced SFG intensity effects from the EDL and used the experimentally derived surface potential to calculate surface densities, ion affinities and surface pH/pOH at alcohol/water interfaces.[30] Recent efforts to quantfy $\chi^{(3)}$ systematically have been led by Geiger and coworkers and others[26, 27, 31-33] who have published mathematical procedures for assessing $\chi^{(3)}$'s impact on SFG line shapes and relative intensities.

In the experiments described below, we considered contributions from a simple $\chi^{(2)}$ response as well as the role played by the static, electric field induced $\chi^{(3)}$ effect. Careful analysis showed that including $\chi^{(3)}$ led to very little change in intensities, line shapes and band positions in the C-H stretching region (2800-3000 cm^{-1}). Slight differences were observed at the lowest GU concentrations but only for the methyl Fermi resonance (2940 cm^{-1}) and the methyl asymmetric stretch (2960 cm^{-1}) features. Our analysis of lipid monolayer structure and organization did not include these features and instead focused on methyl and methylene symmetric stretch transitions at 2872 and 2948 cm^{-1}, respectively. For these spectral bands, changes induced by $\chi^{(3)}$ were indistinguishable from day-to-day experimental uncertainties, thus the data presented below including intensity ratios reflect only a $\chi^{(2)}$ contribution.

The experiments in this work were acquired under three polarization conditions (SF, VIS, IR): SSP, PPP, and SPS. PPP polarization samples all nonzero $\chi^{(2)}$ elements and SPS and SSP only sample a single $\chi^{(2)}$ element. In this analysis, the SSP polarization combination is used to measure film organization.

We note that VSFG has been used previously to perform ex situ measurements of SSA surface composition. Specifically, Geiger and coworkers collected aerosol particles from the Scripps wave flume and then tested the surface for the presence of organic species. They found clear evidence of organic accumulation at these surfaces, but broad lineshapes and a lack of distinctly assigned features led the authors to conclude that natural SSA have heterogeneous alkyl coating on their surfaces.[32, 34]

2.3.1 Vibrational Sum Frequency System at Montana State University

Two different assemblies were used to acquire VSF spectra. At Montana State University, the VSFG assembly is built around a Coherent Libra Ti:Sapphire laser with a 85 fs pulse width and a 1 kHz repetition rate (Figure 1). This amplified system produces 3.3 W of 800 nm light. A beam splitter reflects 80% of this light into a Coherent OPerA Solo optical parametric amplifier that generates the IR light centered at 3.4 μm used in the VSFG measurements. The remaining 20% of the 800 nm output is shaped with a 4-f pulse shaper using a grating (1400 grooves/mm^{-1}) blazed at 800 nm (Spectrogon), a 25 cm FL cylindrical lens and an adjustable slit. This pulse shaper results in resolution that is sub-10 cm^{-1}. Both the IR and visible light polarizations are controlled with waveplates before being focused onto the sample with 10 cm FL lenses. The laser beams must be overlapped spatially and temporally to create the sum frequency signal. This SF signal is reflected using a 10 cm FL off-axis parabolic mirror to collimate the light before focusing the SF signal into a monochromator (SpectraPro-300i, Acton Research Corporation) and then dispersing onto a 1340 x 100 pixel CCD (PIXIS100B, Princeton Instruments). SFG spectra were normalized using the SFG response off of a gold wafer and corrected for background contributions. The 2918 cm^{-1} peak of DMSO[35] was used to calibrate the IR frequency of the SFG signal. Spectral features in the different regions were normalized to the instrument response from a gold substrate so that relative intensities could be compared quantitatively.[36, 37]

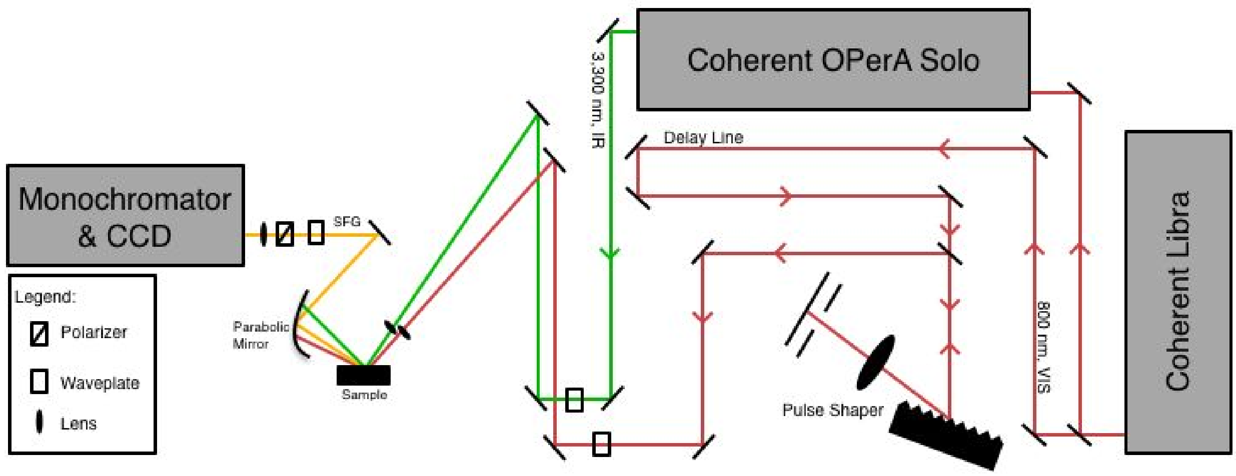

Figure 1. Layout of the MSU SFG system. The pulse shaper is made up of a grating, a 25 cm cylindrical lens, a variable slit, and a mirror.

2.3.2 Scanning Sum Frequency Generation

The SFG spectrometer used to probe O-H vibrations presented in this work has been described elsewhere.[38-42] Briefly, this spectrometer (EKSPLA) utilizes a Nd:YAG laser (EKSPLA PL2251A-50) with a 29 ps pulse at 10 Hz. Part of this fundamental output is converted from 1064 nm to a visible (532 nm) beam. The remaining fundamental is sent to an OPA to produce IR light that is tunable from 650 cm^{-1} to 4300 cm^{-1}. One point to note is that data acquired with the scanning SFG system were not referenced to any external standard so band intensities, especially at the extreme edges of the spectral range covered, were subject to greater uncertainties in their relative concentrations.

2.3.3 Surface Tension

Surface tension measurements were made with a NIMA Langmuir trough (Model 302LL) with a NIMA PS4 pressure sensor and a Micro Processor Interface 104. The Langmuir trough was cleaned with chloroform and Millipore water before use. Paper Wilhelmy plates (Brown Waite Engineering) were used to measure surface tension. This assembly consistently showed an accuracy of (0.4 mN/m) and precision of (0.2 mN/m) using Millipore water (18.2 MΩ-cm) as a standard.

For pressure-area isotherms, the Langmuir trough barriers were closed at a speed of 10 cm^2/min. The surface pressure (π) was measured as a function of surface area. This surface pressure is related to the surface tension of the underlying neat liquid phase (γ_0) and the surface tension of the subphase and a surfactant monolayer (γ).

$$\pi = \gamma_0 - \gamma \qquad (2)$$

For ideal mixed monolayers containing two species that are restricted to the surface, intermolecular interactions can be quantified by calculating the excess free energy of mixing, ΔG_{mix}^{E}. This free energy, shown in Equation 3, is dependent on A_{12}, which is the measured area per molecule of a mixed monolayer, A_1 and A_2, which are the area per molecule of a pure monolayer of one of the species in the mixed monolayer, and x_1 and x_2 which are the mole fractions of each of the species in the mixed monolayer.[43, 44]

$$\Delta G_{mix}^{E} = \int_{\pi_1}^{\pi_2} N_A (A_{12} - x_1 A_1 - x_2 A_2) d\pi \qquad (3)$$

While the surface films examined in these studies consisted of an insoluble lipid and a highly soluble saccharide, treating these systems as mixed monolayers afforded us the opportunity to assess how cooperative adsorption affected surface free energy.

2.3.4 Differential Scanning Calorimetry

Differential scanning calorimetry (DSC) measurements were made using a TA Instruments Discovery (New Castle, DE). For these experiments, sealed Tzero pans and Tzero hermetic lids (TA Instruments) were equilibrated at 20°C. Following equilibration, the pans were heated by 0.5°C/min until 55°C to capture the transition temperature T_m of DPPC at approximately 41°C.

Vesicle solutions were made using standard protocols.[45] Briefly, a ~1 mg/ml solution of DPPC in chloroform was prepared in a round bottom flask. The chloroform was removed with a rotary evaporator with a bath temperature that was ~10°C greater than T_m of DPPC. The remaining lipid film was rehydrated with either Millipore water or 100 mM pH 9.0 carbonate buffer and then sonicated for 30 minutes in a bath that was ~10°C greater than the T_m. The vesicle solutions were then mixed into GU solutions in the appropriate solvent (Millipore water or 100 mM pH 9.0 carbonate buffer) producing a vesicle solution that was 10 mM DPPC. These solutions were left to equilibrate for ≥ 8 hours before use.

3. RESULTS AND DISCUSSION

3.1 High Concentration Glucosamine

3.1.1 Surface Tension and Free Energy Measurements

Figure 2 shows pressure-area isotherms for DPPC on solutions having different concentrations of glucuronic acid. We note here that GU itself is not surface active. The surface tension of GU containing aqueous solutions showed no dependence on GU concentration (the measured surface tension of a 50 mM GU solution was 73.2 ± 0.4 mN/m at 21˚C). The pH of these bulk solutions containing GU is 3.3. The most notable isotherm in Figure 2 is from DPPC on a 50 mM GU solution. This isotherm characteristically has higher surface pressures (π) at all surface coverages of DPPC compared to the other isotherms shown. At a given area, a higher π requires the system's surface tension to be lower than the reference, consistent with the hypothesis that the DPPC film is drawing additional material to the interface from bulk solution.

Another feature of the DPPC-on-50-mM-GU isotherm in Figure 2 is the change in slope at 41 mN/m. Similar behavior has been observed previously in DPPC/fibrinogen[46] and in DPPC/DPPG mixtures mixed with recombinant surfactant-associated protein C (SP-C);[47] this result has been interpreted as the solute being 'squeezed' out of the insoluble Langmuir film leading to a higher isothermal compressibility. This slope-change is evident, but much less pronounced in the sub-50 mM isotherms. By forcing GU out of the monolayer, the 50 mM isotherm at high pressures approaches behavior similar to that of other isotherms from solutions having lower GU concentrations. With the DPPC molecules approaching the collapse pressure of the monolayer one expects little impetus for the (deprotonated) glucuronic acid to remain coordinated with insoluble DPPC monomers.

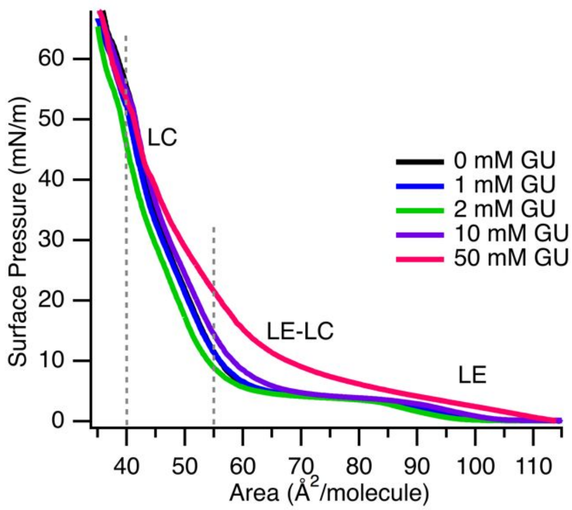

Figure 2. π-A isotherms of DPPC on various concentrations of GU at room temperature (21 °C). Vertical dotted lines correspond to 40 and 55 Å^2/mol DPPC surface coverage which is the surface coverage VSFG measurements were taken.

Isotherm data in Figure 2 can be used to quantify the effects of cooperative adsorption on surface thermodynamics. For excess free energy of mixing calculations, Equation 3 is simplified with the following approximations: first, DPPC is assumed to be the only species constrained to the aqueous/vapor interface. Species 2, GU, is not surface active by itself given the invariance of the surface tension to GU bulk concentration. With these assumptions, Equation 3 becomes:

$$\Delta G_{mix}^{E} = \int_{\pi_1}^{\pi_2} N_A (A_{12} - A_1) d\pi \quad (4)$$

The excess of free energy of mixing is plotted against surface pressure in Figure 3. In an ideal mixed monolayer, a negative ΔG_{mix}^{E} indicates attractive interactions between the components of the monolayer and signifies a more stable monolayer.[44] In this limit, DPPC on 1 and 2 mM solutions of GU are more condensed and are stabilized. For higher GU concentrations, because the mixing is not ideal, stability criteria need to change to account for the sign change in the excess free energy. The positive ΔG_{mix}^{E} for the 10 and 50 mM GU sub-phases is a result of the DPPC molecules being more 'expanded' than the ideal pure DPPC phase. For 'expanded' monolayers, at any given surface area, the surface pressure is greater and thus the surface tension of the mixed solution is lower. One possible mechanism for this lower surface tension is that GU, at higher concentrations, replaces the water at the surface because of Coulomb interactions with the DPPC head group (further evidence for water replacement by GU is shown in the DSC results in section 3.1.4). This surface tension lowering at higher saccharide concentrations (≥10 mM) serves as evidence supporting cooperative adsorprtion as a possible source of soluble organics in SSA given that lower surface tensions have been correlated to a greater activation of primary marine aerosols.[14]

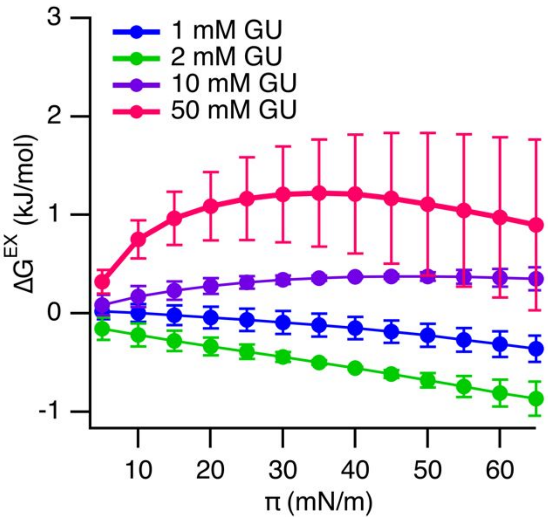

Figure 3. Excess free energy of mixing for DPPC on aqueous GU solutions. The reported errors correspond to the standard deviation of 2-3 independent π-A isotherms.

3.1.2 C-H VSFG

Figure 4 shows VSFG spectra acquired from DPPC films on a pure Millipore water solution (top) and on a 50 mM GU solution (bottom). The left and right columns correspond to DPPC surface coverage of 55 Å^2/molecule and 40 Å^2/molecule, respectively. Each panel of Figure 4 contains VSFG spectra acquired under symmetry allowed VSFG polarization combinations (SSP, SPS and PPP; PSS data not included). Of note in all spectra are the relative intensities of the methyl symmetric stretch at 2872 cm^{-1} (r^+) and the methylene symmetric stretch at 2848 cm^{-1} (d^+).[48, 49] Frequently, the intensity ratio, r^+/d^+, is used as a measure of relative order within organic monolayers studied with VSFG in an SSP polarization configuration.[19, 50-52] P-polarized infrared light probes those vibrations having their IR transition moment aligned primarily along the surface normal. Consequently, a tightly packed monolayer with upright alkyl chains will show a large r^+ response from the methyl groups directed away from the subphase and a weak or nonexistent d^+ response due in part to the d^+ transition moment being aligned in the surface plane and also because of local inversion symmetry found in all-*trans* chains. A consequence of this monolayer organization is a large r^+/d^+ ratio that can be ≥ 20.[50] At lower surface coverages, alkyl chains become more disordered with *gauche* defects that diminish the r^+ signal and give rise to a larger d^+ response. While the r^+/d^+ ratio has never been correlated quantitatively with any sort of order/disorder parameter, it nevertheless serves as a useful tool for qualitatively assessing monolayer organization.

Looking first at the more expanded DPPC monolayer (55 Å^2/molecule, first column), one observes that the d^+ band is relatively large implying a high degree of chain disorder as evidenced by an r^+/d^+ ratio of less than unity. These results are consistent with similar findings reported by Allen, *et al.*[19] Addition of GU to the aqueous subphase causes changes in the spectra, most notably by enhancing r^+ intensity so that when aqueous GU concentrations exceed 10 mM (lower left panel, Figure 4), the r^+/d^+ ratio has risen from 0.5 (at 0.0 mM GU) to > 1, showing that chains have adopted a more upright orientation. Interestingly, the origin of this change appears to be growth of the r^+ intensity rather than a decrease in d^+ intensity

A second change in the 55 Å^2/molecule DPPC spectra occurs with the SPS polarization. On a water subphase, the peak at 2960 cm^{-1} assigned to a CH_3 asymmetric stretch (r^-) is almost non-existent (top left panel, Figure 4). On an aqueous subphase containing 50 mM, however, the r^- vibrational band is quite strong. The presence of this vibrational signal in the plane of the surface can result from structural and/or dynamic changes in the DPPC monolayer. Certainly, a larger r^+ feature observed in the SSP spectra implies a more upright lipid chain orientation leading one to also expect a larger r^- response in the SPS spectrum. However, the literature also contains numerous examples where a large r^+ response *does not* always correlate with large r^- signal for reasons related to molecular dynamics. Rapid internal rotation of a methyl group about its C_3 axis will preferentially suppress VSFG signal from r^- relative to r^+.[53] We propose that the strong r^- response observed in expanded DPPC monolayers on a 50 mM GU solution is due to condensation of DPPC monomers induced by GU solutes that have cooperatively adsorbed to the aqueous/vapor interface. Such condensation would restrict methyl rotation and allow the r^- transition to acquire appreciable intensity in the SPS VSFG spectrum.

In tightly packed DPPC monolayers (40 Å^2/molecule, right column in Figure 4), changes in monolayer organization as a function of aqueous GU concentration are more subtle. At higher GU concentrations, d^+ intensity increases compared to the d^+ intensity of tightly packed DPPC on pure water. Figure 5 shows the r^+/d^+ ratios for both the expanded 55 Å^2/molecule and the tightly packed 40 Å^2/molecule. In the 55 Å^2/molecule data, an increase in the ratio as the GU concentration increases supports the idea that GU is changing the DPPC organization at the surface. In the 40 Å^2/molecule data, where the data show an initial drop in this ordering, changes in organization are attributed to a change in overall molecular tilt, given that the DPPC acyl chains themselves should already be in all-trans configurations with very little free area available to reorganize conformational structure. This ratio then increases with additional GU and with 100 mM GU in the subphase, the ratio returns to a value close to that of DPPC on pure water. In both cases – expanded and tightly packed – changes in the VSFG spectrum resulting from GU in the aqueous subphase support a cooperative adsorption mechanism.

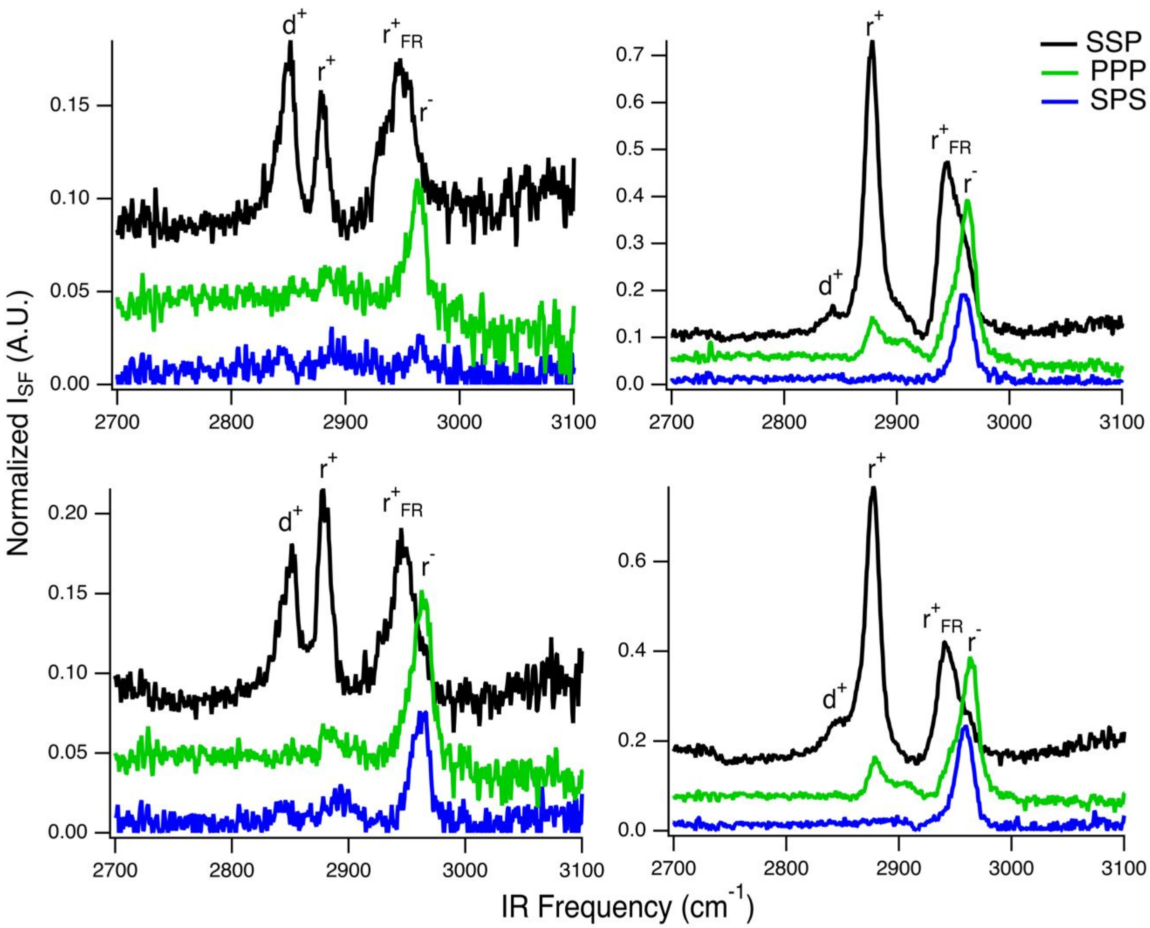

Figure 4. SF spectra of DPPC. The top row is DPPC on water and the bottom row is on a 50 mM GU solution. The left column has a surface coverage of 55 Å^2/molecule DPPC and the right 40 Å^2/molecule DPPC. GU is deprotonated, resulting in an ionic strength of the bulk solution that is equal to the concentration of GU. The pH of GU containing solutions is controlled GU, which has a pKa of 3.20. [18]

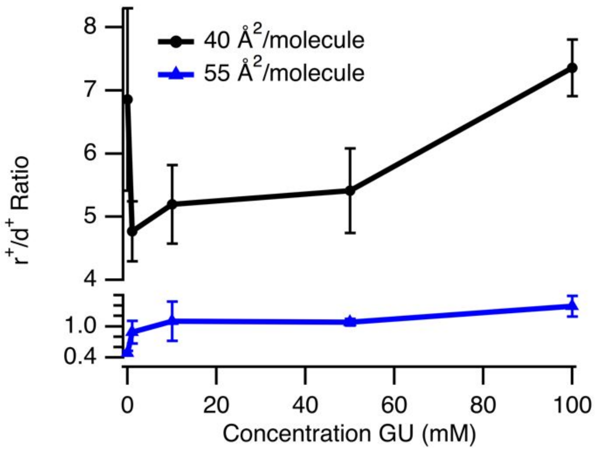

Figure 5. Ratio of the CH_3 symmetric stretch (r^+) to the CH_2 symmetric stretch (d^+). For each GU concentration, data was averaged over four data acquisitions on a single day. The reported error is the standard deviation of this averaged data from 2-4 different independent experiments.

3.1.3 OH Vibrational Region

To further examine GU induced changes to DPPC monolayer organization, spectra were acquired in the O-H stretching region. Figure 6 shows VSFG spectra covering an expanded IR frequency range and acquired from expanded DPPC monolayers (55 $Å^2$/molecule) as a function of GU concentration. The IR frequency range now covers the 3000 – 3700 cm^{-1} and is dominated by broad vibrational resonances. The feature at 3250 cm^{-1} has been attributed to tetrahedrally hydrogen bound water molecules or coupled hydrogen bond donors. The feature at 3400 cm^{-1} is typically assigned to asymmetrically hydrogen bound water molecules or loosely coordinated water molecules such as those found in liquid water. The first observation from data in Figure 6 is that addition of GU to the aqueous subphase changes the structure of interfacial water. There is a shift in the maximum water intensity from the 3400 cm^{-1} peak to the 3250 cm^{-1} peak in the spectrum of DPPC on 1 mM GU compared to the spectra of DPPC on pure water. This shift in intensity from 3400 cm^{-1} to 3250 cm^{-1} indicates an increase in the *relative* amount tetrahedrally hydrogen bound water molecules. Second, the *total* intensity in the –OH stretching region diminishes as GU concentration increases. This reduced intensity can be a result of fewer water molecules in the anisotropic interfacial region or from a more randomly organized surface. Given that the interface has a significant amount of formal charge (from the DPPC headgroups and any negatively charged GU) *and* given the observed shift in vibrational intensity from disordered water (at 3400 cm^{-1}) to ordered water (at 3250 cm^{-1}), a more randomized surface structure is unlikely. Instead, we propose that the observed reduction in overall water intensity is due to GU cooperatively adsorbing to the lipid surface, diminishing the width of the double layer and, by extension, reducing the width of the anisotropic region containing water molecules that contribute to a VSFG spectrum. Similar results are observed for the 40 $Å^2$/molecule DPPC film as well, although the magnitude of these changes is much less pronounced.

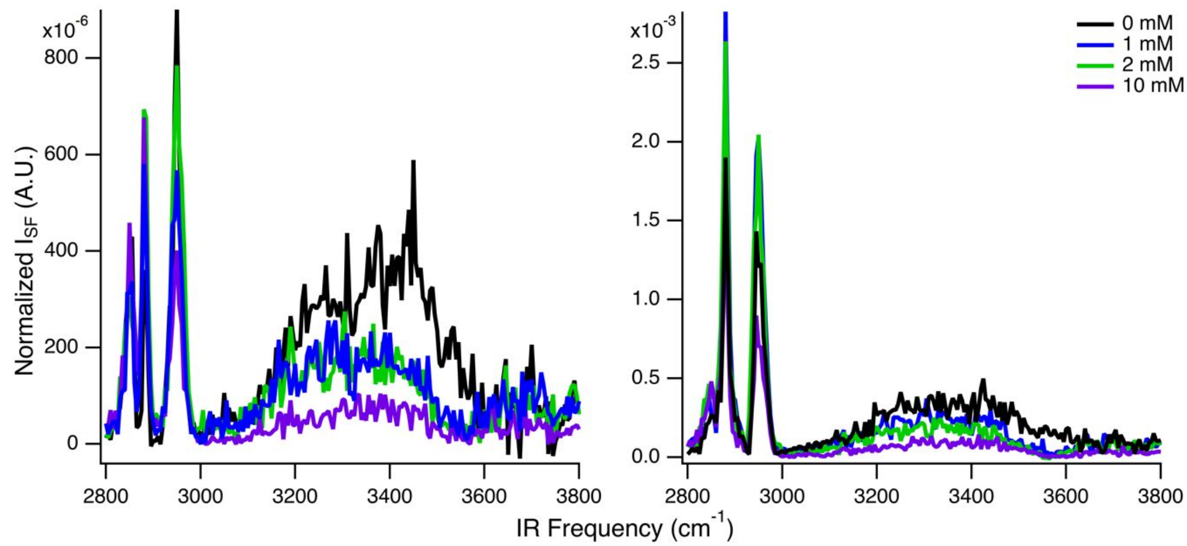

Figure 6. O-H vibrational region for 55 Å^2/molecule DPPC (left) and 40 Å^2/molecule DPPC (right) on various concentrations of GU/Millipore solutions. In these experiments, the SFG spectrometer was optimized to collect data in the O-H stretching region and CH band intensities are subject to larger uncertainties than in Figure 4.

3.1.4 Consequences of GU association with DPPC Bilayers

Glucuronic molecules adsorb cooperatively to lipid monolayers at the aqueous/air interface likely displacing water molecules and – we believe – shrinking the double layer that contains water structured by the lipid headgroups. To search further for signs of this saccharide-lipid association, DPPC vesicles were prepared in a buffered aqueous solution. After vesicle formation, GU was introduced to solution and the effects of GU addition on bilayer structure were tested with differential scanning calorimetry. The main transition of the DPPC bilayers is the phase change from a gel to a liquid crystalline state at 40.4 ˚C. There is an additional phase transition below the main transition, forming a "ripple phase", in which a flat membrane in the gel phase becomes a periodically undulated bilayer.[54] The presence of GU in the lipid vesicle solution results in three significant changes to the DPPC vesicle endotherm. First, the data show a linear increase in the T_m as the concentration of GU added to the vesicle solution is increased. This linear trend is reminiscent of colligative properties that change with increasing solute concentration. In bulk solution, colligative properties result from a reduction of a liquid's chemical potential because of the presence of a solute.

The second significant change to the DSC endotherms is that the DPPC phase transition from gel to liquid crystalline phase splits into two distinct melting temperatures with a weaker peak appearing in the endotherm at temperatures 1-2˚C higher than the main transition. The introduction of a second peak in lipid endotherms has been reported previously and attributed to dehydration of the vesicles' lipid head groups.[55] This dehydration mirrors the trend in the DPPC isotherm on 50 mM of glucuronic acid where there is evidence that GU may be replacing water molecules at the surface and creating a lower surface tension. Additional evidence of this dehydration appears in the VSFG spectra where contributions from water in the OH stretching region diminish with increasing GU concentration. This second T_m, labeled T_{m2}, also increases linearly in temperature with glucuronic acid concentration. Other instances of a second, distinct peak in PC lipids, have occurred with divalent and trivalent cations. These ions are expected to be located at the bilayer surface—interacting with the headgroup's negatively charged phosphate[56] and are expected to have significant effects on the lipid packing due to rearrangement of the zwitterionic headgroup region, resulting in a more condensed monolayer.[57] To our knowledge, data shown in Figure 7 are the first to show this effect with cooperatively adsorbed *anions*. With the growth of the second peak at the expense of the first peak, ΔH_{cal} has not significantly changed between the original and new peak.[56, 57]

GU, in concentrations >50 mM, results in a loss of the ripple phase transition, labeled T_p (pretransition temperature). Prior studies have shown that T_p for phosphatidylcholines (PCs) is scarcely affected by moderate concentrations (1 M) of monovalent cations K^+ and Na^+. With divalent cations (1 M Mg^{2+} and Ca^{2+} (> 10 mM)), T_p increases. Additionally, Ca^{2+} concentrations above 1 mM have reduced ΔH_{cal} of the pretransition, but the ΔH_{cal} increases with Ca^{2+} concentrations above 10 mM. Data in Figure 7 show an entirely different result compared to divalent cation-induced condensing effects on T_m.

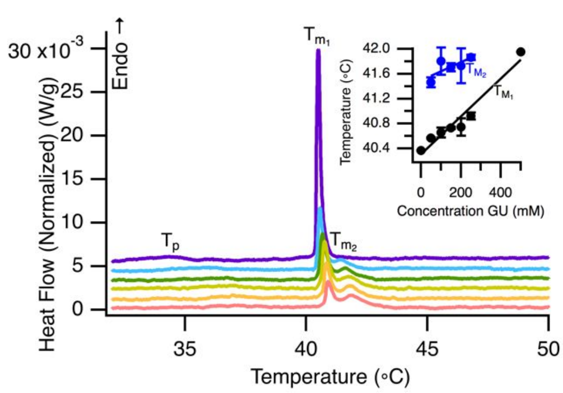

Figure 7. DSC measurements for DPPC vesicles in Millipore solutions with GU. All transitions are endothermic. The concentration of GU increases by 50 mM successively from top (0 mM) to bottom (250 mM) trace. Peak temperatures for both the T_{m1} and T_{m2} transitions are plotted in the inset. Error bars are calculated from the standard deviation from three measurement.

3.2 Buffers

VSFG, Langmuir trough and DSC measurements described in Section 3.1 all support a cooperative adsorption mechanism between DPPC and glucuronic acid solutes in solutions made from Millipore water (pH = 5.8). Data presented in the previous sections show that GU condenses expanded DPPC films and forces a reorganization of the lipid acyl chains. While the mechanism responsible for DPPC-GU association remains unconfirmed, the most probable explanation is Coulomb attraction between the negatively charged GU and DPPC’s positively charged quaternary ammonium group. This Coulomb attraction appears to partially dehydrate the lipid headgroup, a result that is consistent with DSC data shown in Figure 7 (for DPPC vesicles in GU-containing aqueous solution) and VSFG data shown in Figure 6. Whether such interactions remain important under environmentally relevant conditions is a question that must be addressed before cooperative adsorption can be considered as a strong driving force responsible for organic enrichment in the sea-surface microlayer. Specifically, oceans are buffered to a pH of 8.1 due primarily to dissolved carbonate/bicarbonate species.

Furthermore, ocean water generally has high ionic strength (~0.7M) comprised primarily of monovalent and divalent cations as well as Cl^-, and SO_4^{2-}. Experiments described in the following section examine the impact of a carbonate buffer (pH = 9.0) on GU's cooperative adsorption to DPPC monolayers. Data suggest that sufficiently high ionic strengths will impede DPPC-GU association and limit cooperative adsorption.

3.2.1 Surface Tension and Excess Free Energy of Mixing

Isotherm data from DPPC monolayers on buffer solutions do not differ significantly with GU concentrations ≤ 10 mM (Figure 8). Unlike the unbuffered case (Figure 2) where the addition of GU led to measurable changes in surface pressure at given DPPC surface coverages, surface pressure data from DPPC on buffer solutions at the same coverages (40 Å^2/DPPC and 55 Å^2/DPPC) are virtually identical. Only when GU concentration is increased to 50 mM does isotherm behavior change significantly, again becoming more expanded similar to the observed behavior for DPPC monolayers on unbuffered solutions containing GU. If Coulomb attractions were responsible for cooperative GU adsorption to DPPC monolayers from unbuffered aqueous solutions, then one might reasonably expect the excess carbonate/bicarbonate ions in the buffered solutions to fulfill the same function. Such interactions would make the monolayer's structure and organization largely insensitive to GU concentration. When GU concentration reaches half of the buffer concentration, GU causes an expansion of the DPPC monolayer and a corresponding reduction in the surface tension in the system—paralleling the effects of GU at 10 and 50 mM in the unbuffered cases.

The pressure-area isotherms in Figure 8 show two slope changes in the liquid condensed phase at ~45 mN/m and ~55 mM/m. The presence of these slope changes with no GU present in the subphase indicates that any 'squeeze-out' effects would be from buffer ions being squeezed out of the DPPC monolayer in the 0 mM GU case. For the GU containing subphases, attributing any 'squeeze-out' effects to either the buffer or GU is difficult. With the 50 mM GU subphase, these slope changes are the more pronounced than in the other π-Area isotherms and these changes occur at lower surface pressure. The lower surface pressure of these 'squeeze-out' effects is reminiscent of the proposed 'solute expulsion' observed in the 50 mM GU/Millipore samples and this may indicate GU being preferentially removed from the monolayer relative to carbonate.

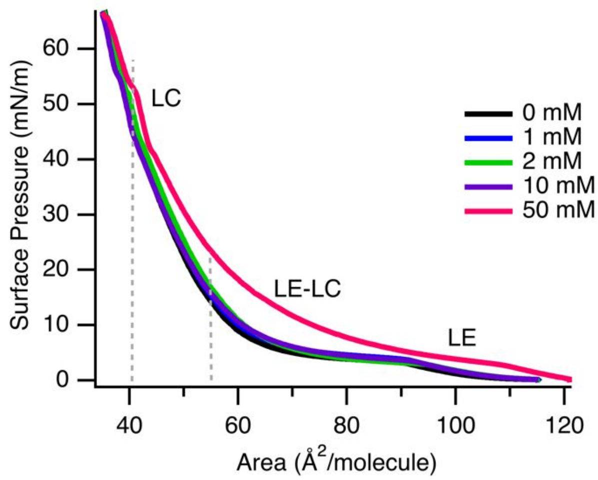

Figure 8. π-A isotherms of DPPC on various concentrations of GU in pH 9.0 buffer (sodium carbonate and sodium bicarbonate) at room temperature (21 °C). Vertical dotted lines correspond to 40 and 55 Å^2/mol DPPC surface coverage which is the surface coverage VSFG measurements were taken.

For the excess free energy of mixing calculations, the same approximations as in the water solution were made. For the three lower concentrations of GU used (1, 2, 10 mM) the excess free energy of mixing is negative. This indicates that adding GU to the subphase results in a more stable monolayer. In the case of the 50 mM GU/buffer solution, the area/molecule is expanded and the system's surface tension is lowered. This surface tension lowering again indicates the GU is in sufficiently high concentration relative to the buffer to competitively associate with the lipid monolayer and disrupt lipid headgroup solvation. Field studies of the sea surface microlayer (SSML) have shown saccharide concentrations is in considerable excess relative to bulk,[8] so the cooperative adsorption mechanism may still be a relevant pathway for soluble organic accumulation in SSA.

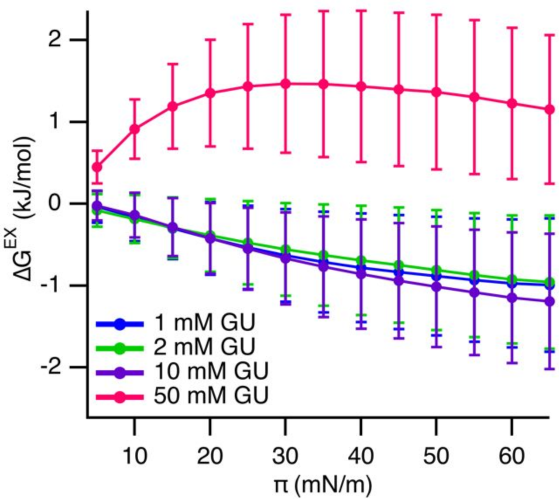

Figure 9. Free energy of mixing for DPPC on Buffers. The reported errors correspond to the standard deviation of 2-3 independent π-A isotherms.

3.2.2 C-H VSFG

Isothermal data in Figures 8 and 9 support observations from VSFG experiments performed on the same systems. Similar to Figure 4, Figure 10 shows VSFG spectra from DPPC films on a pure buffered subphase (top) and on a buffered subphase containing 10 mM GU solution (bottom). The left and right columns correspond to DPPC surface coverages of 55 Å^2/molecule and 40 Å^2/molecule, respectively. Each panel of Figure 10 contains VSFG spectra acquired under symmetry allowed VSFG polarization combinations (SSP, SPS and PPP; PSS data not included). Again, the relative intensities of the methyl symmetric stretch at 2870 cm^{-1} (r^+) and the methylene symmetric stretch at

2840 cm^{-1} (d^+) are the relevant quantities used to assess lipid film structure and organization.

Lipid organization in 40 Å^2/molecule films shows very little dependence on GU concentration from 0 mM to 10 mM GU in pH 9 buffered solutions. In contrast to changes observed on unbuffered solutions where the r^+/d^+ ratio diminishes from 7.0 to 4.8 with small additions of GU, adding GU to buffered solutions results in the tightly packed DPPC r^+/d^+ ratio changing from 5.6 to 7.0 (Figure 11). We surmise that if Coulomb attractions were the driving force behind GU cooperative adsorption in unbuffered solutions, then these interactions will be suppressed by the higher ionic strength buffer. Reduced Coulomb attraction between GU and DPPC means that DPPC monolayer organization should be insensitive to GU bulk concentration and the r^+/d^+ ratio should not change significantly.

In the 55 Å^2/molecule data, the ratio for the solutions containing GU is slightly but measurably higher than the solutions that do not contain GU (Figure 11). More importantly, organization in these expanded monolayers on buffered solutions is significantly enhanced (with and without GU) compared to similar DPPC coverages on Millipore water. Together, these results imply that GU may cooperatively adsorb weakly to more expanded DPPC monolayers on alkaline solutions but most of the lipid monolayer organization is controlled by the inorganic carbonate/bicarbonate species.

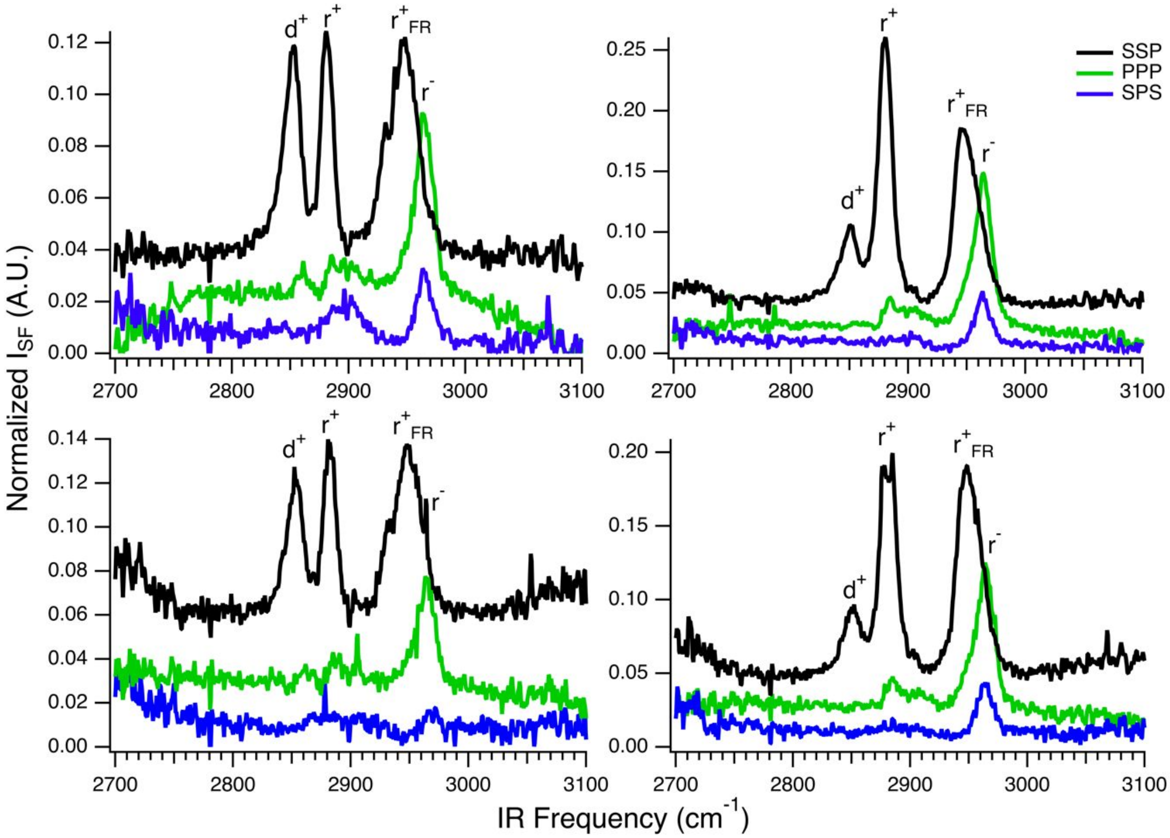

Figure 10. SF spectra of DPPC with a pH 9.0 buffer subphase. The top row is DPPC on a 100 mM carbonate buffer ((buffer ionic strength is 400 mM) with no glucuronic acid and the bottom row is on a 100 mM carbonate buffer with 10 mM GU. The left column has a surface coverage of 55 Å^2/molecule DPPC and the right 40 Å^2/molecule DPPC.

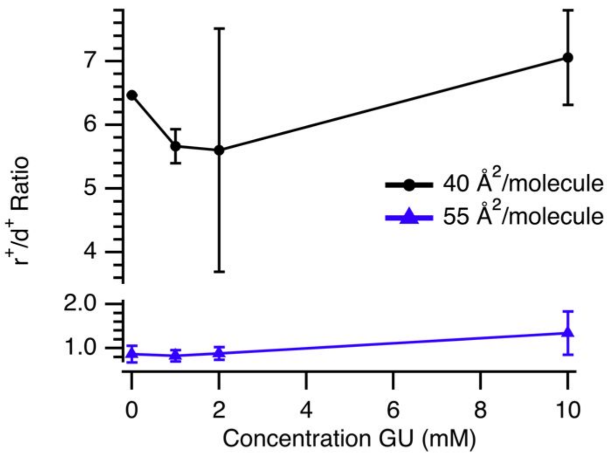

Figure 11. r+/d+ ratios for DPPC on buffers. For each GU concentration, data was averaged over four data acquisitions on a single day. The reported error is the standard deviation of this averaged data from three different independent measurements.

3.2.3 OH Stretch

The OH vibrational spectra on buffer solutions show similar intensities for the OH stretching region regardless of GU concentration (Figure 12). In all instances including solutions that do not contain GU, the free OH peak is nonexistent and the spectral intensity in the hydrogen bonded region is significantly diminished compared to similar spectra acquired from DPPC monolayers on Millipore water. Again, these findings support a picture where carbonate/bicarbonate ions strongly associate with the DPPC headgroups leaving GU with little opportunity to cooperatively adsorb to the aqueous interface. The peaks at 3200 and 3400 cm^{-1} are all similar in intensity showing that changes in GU concentration is not causing significant changes to the surface water structure because the much higher concentration of buffer ions mitigates any affect from the GU ions.

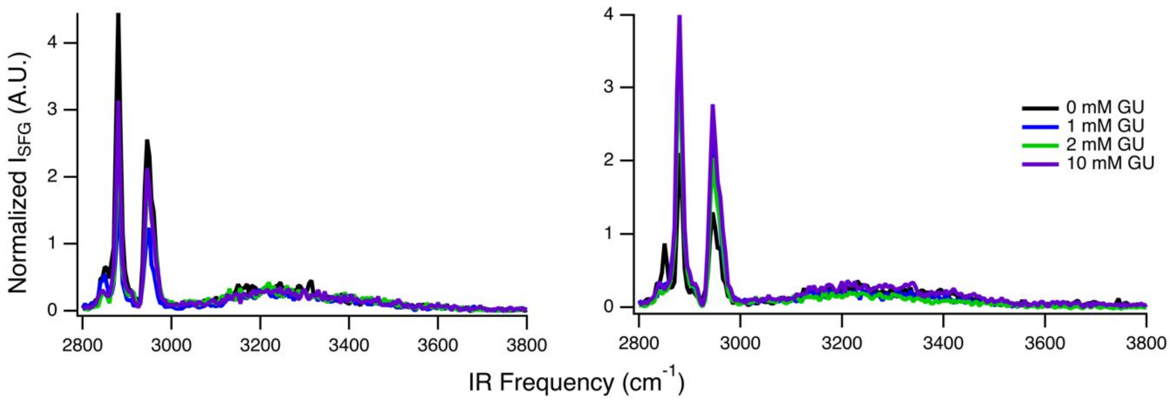

Figure 12. O-H vibrational region for 55 Å^2/molecule DPPC (left) and 40 Å^2/molecule DPPC (right) on various concentrations of GU in pH 9.0 carbonate buffer.

3.2.4 Lipid Bilayers in Buffered Solution

For the lipid vesicles in buffer solution, the first two concentrations, 0 mM and 50 mM GU, fall within the solution's buffering capacity (Figure 13). By 100 mM GU, the pH of the vesicle solution is reduced to 7 and for 250 mM GU, the vesicle-containing solution pH is again 3.3. Once the GU concentration is greater than the buffer, the second phase transition reappears (T_{m2}), the pretransition temperature disappears, and the T_m increases linearly with GU concentration. These same effects were observed in the DSC results from vesicles in unbuffered Millipore water, leading us to propose that competition between the buffer ions and the GU ions is responsible for changing phase transition behavior in the bilayers.

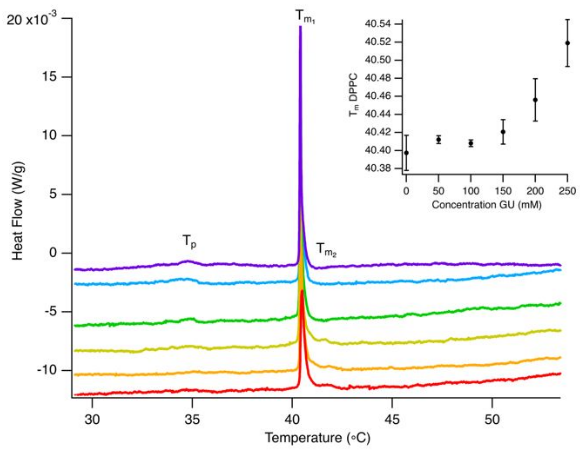

Figure 13. DSC measurements for DPPC vesicles in buffer solutions with GU. All transitions are endothermic. The concentration of GU increases by 50 mM successively from top (0 mM) to bottom (250 mM) trace. Peak temperature for T_{m1} transition is plotted in the inset. Error bars are from the standard deviation of three measurements.

4. CONCLUSIONS

Experimental studies described in this work show that the negatively charged monosaccharide, glucuronic acid, causes structural changes to moderately packed DPPC films and alters phase behaviors of these films. Specifically, larger concentrations of GU, 50 mM, show a larger footprint (area/molecule) in surface tension measurements which we believe is due to cooperatively adsorbed solutes to the lipid monolayer. Differential scanning calorimetry results also show a dehydration effect resulting in a second transition in the DPPC monolayer. This cooperative adsorption of GU to the DPPC film is competitive when there are buffer ions present in greater abundance than the GU solutes. As shown in the SFG and surface tension data, when the concentration of buffer is 10x greater than the concentration of GU, few changes are seen to DPPC organization. When GU concentration reaches 50% of buffer concentration, we see an expansion of the DPPC footprint in surface tension measurements that is similar to the data in the pure water measurements. In the DSC measurements, we see GU associated phase changes when the GU concentration is equal to the buffer concentration. These results show that anions can have a significant effect on film organization even though there is a competition for available charge sites at the interface. The changes in surface tension, even with competition from buffer ions, add support to cooperative adsorption being a mechanism for increased organic content at the surface.

ACKNOWLEDGEMENTS

Material presented in this manuscript is based in part upon work supported by the National Science Foundation EPSCoR Cooperative Agreement OIA-1757351. A portion of the research was performed using the William R. Wiley Environmental Molecular Science Laboratory (EMSL), a U.S. Department of Energy's Office of Science User Facility sponsored by the Office of Biological and Environmental Research and located at Pacific Northwest National Laboratory (EMSL user proposal 48281). The authors also acknowledge support from the Montana Research and Economic Development Initiative

(M-REDI). A.T. acknowledges support by the US Department of Energy (DOE), Office of Science, Office of Basic Energy Sciences, Division of Materials Science and Engineering.

The authors declare no competing financial interests.

REFERENCES

1. Fossum, K. N.; Ovadnevaite, J.; Ceburnis, D.; Dall'Osto, M.; Marullo, S.; Bellacicco, M.; Simo, R.; Liu, D.; Flynn, M.; Zuend, A.; O'Dowd, C., Summertime Primary and Secondary Contributions to Southern Ocean Cloud Condensation Nuclei. *Sci. Rep.* **2018,** *8* (1), 13844.

2. Russell, L. M.; Hawkins, L. N.; Frossard, A. A.; Quinn, P. K.; Bates, T. S., Carbohydrate-Like Composition of Submicron Atmospheric Particles and their Production from Ocean Bubble Bursting. *Proc. Natl. Acad. Sci. U. S. A.* **2010,** *107* (15), 6652-6657.

3. Wilson, T. W.; Ladino, L. A.; Alpert, P. A.; Breckels, M. N.; Brooks, I. M.; Browse, J.; Burrows, S. M.; Carslaw, K. S.; Huffman, J. A.; Judd, C.; Kilthau, W. P.; Mason, R. H.; McFiggans, G.; Miller, L. A.; Najera, J. J.; Polishchuk, E.; Rae, S.; Schiller, C. L.; Si, M.; Temprado, J. V.; Whale, T. F.; Wong, J. P.; Wurl, O.; Yakobi-Hancock, J. D.; Abbatt, J. P.; Aller, J. Y.; Bertram, A. K.; Knopf, D. A.; Murray, B. J., A Marine Biogenic Source of Atmospheric Ice-Nucleating Particles. *Nature* **2015,** *525* (7568), 234-238.

4. Meskhidze, N.; Xu, J.; Gantt, B.; Zhang, Y.; Nenes, A.; Ghan, S. J.; Liu, X.; Easter, R.; Zaveri, R., Global Distribution and Climate Forcing of Marine Organic Aerosol: 1. Model Improvements and Evaluation. *Atmos Chem Phys* **2011,** *11* (22), 11689-11705.

5. Hawkins, L. N.; Russell, L., Polysaccharides, Proteins, and Phytoplankton Fragments: Four Chemically Distinct Types of Marine Primary Organic Aerosol Classified by Single Particle Spectromicroscopy. *Adv Meteorol* **2010,** *2010* (3642), 14.

6. Burrows, S. M.; Ogunro, O.; Frossard, A. A.; Russell, L. M.; Rasch, P. J.; Elliott, S. M., A Physically Based Framework for Modeling the Organic Fractionation of Sea Spray Aerosol from Bubble Film Langmuir Equilibria. *Atmos Chem Phys* **2014,** *14* (24), 13601-13629.

7. Grythe, H.; Strom, J.; Krejci, R.; Quinn, P.; Stohl, A., A Review of Sea-Spray Aerosol Source Functions Using a Large Global Set of Sea Salt Aerosol Concentration Measurements. *Atmos Chem Phys* **2014,** *14* (3), 1277-1297.

8. Jayarathne, T.; Sultana, C. M.; Lee, C.; Malfatti, F.; Cox, J. L.; Pendergraft, M. A.; Moore, K. A.; Azam, F.; Tivanski, A. V.; Cappa, C. D.; Bertram, T. H.; Grassian, V. H.; Prather, K. A.; Stone, E. A., Enrichment of Saccharides and Divalent Cations in Sea Spray Aerosol During Two Phytoplankton Blooms. *Environ. Sci. Technol.* **2016,** *50* (21), 11511-11520.

9. Pham, D. Q.; O'Brien, R.; Fraund, M.; Bonanno, D.; Laskina, O.; Beall, C.; Moore, K. A.; Forestieri, S.; Wang, X. F.; Lee, C.; Sultana, C.; Grassian, V.; Cappa, C. D.; Prather, K. A.; Moffet, R. C., Biological Impacts on Carbon Speciation and Morphology of Sea Spray Aerosol. *ACS Earth Space Chem.* **2017,** *1* (9), 551-561.

10. Facchini, M. C.; Rinaldi, M.; Decesari, S.; Carbone, C.; Finessi, E.; Mircea, M.; Fuzzi, S.; Ceburnis, D.; Flanagan, R.; Nilsson, E. D.; de Leeuw, G.; Martino, M.; Woeltjen, J.; O'Dowd, C.

D., Primary Submicron Marine Aerosol Dominated by Insoluble Organic Colloids and Aggregates. *Geophys. Res. Lett.* **2008,** *35* (17).

11. Burrows, S. M.; Gobrogge, E.; Fu, L.; Link, K.; Elliott, S. M.; Wang, H.; Walker, R., OCEANFILMS-2: Representing Coadsorption of Saccharides in Marine Films and Potential Impacts on Modeled Marine Aerosol Chemistry. *Geophys. Res. Lett.* **2016,** *43* (15), 8306-8313.

12. Link, K. A.; Hsieh, C. Y.; Tuladhar, A.; Chase, Z.; Wang, Z. M.; Wang, H. F.; Walker, R. A., Vibrational Studies of Saccharide-Induced Lipid Film Reorganization at Aqueous/Air Interfaces. *Chem Phys* **2018,** *512*, 104-110.

13. Elliott, S.; Burrows, S.; Cameron-Smith, P.; Hoffman, F.; Hunke, E.; Jeffery, N.; Liu, Y.; Maltrud, M.; Menzo, Z.; Ogunro, O.; Van Roekel, L.; Wang, S.; Brunke, M.; Jin, M.; Letscher, R.; Meskhidze, N.; Russell, L.; Simpson, I.; Stokes, D.; Wingenter, O., Does Marine Surface Tension Have Global Biogeography? Addition for the OCEANFILMS Package. *Atmosphere* **2018,** *9* (6), 216-232.

14. Han, Z. W.; Li, J. W.; Yao, X. H.; Tan, S. C., A Regional Model Study of the Characteristics and Indirect Effects of Marine Primary Organic Aerosol in Springtime Over East Asia. *Atmos Environ* **2019,** *197*, 22-35.

15. Plant, A. L., Supported Hybrid Bilayer Membranes as Rugged Cell Membrane Mimics. *Langmuir* **1999,** *15* (15), 5128-5135.

16. Sackmann, E., Supported Membranes: Scientific and Practical Applications. *Science* **1996,** *271* (5245), 43-48.

17. Ahmed, S. N.; Brown, D. A.; London, E., On the Origin of Sphingolipid/Cholesterol-Rich Detergent-Insoluble Cell Membranes: Physiological Concentrations of Cholesterol and Sphingolipid Induce Formation of a Detergent-Insoluble, Liquid-Ordered Lipid Phase in Model Membranes. *Biochemistry* **1997,** *36* (36), 10944-10953.

18. Bhattacharyya, L.; Rohrer, J. S., *Applications of Ion Chromatography for Pharmaceutical and Biological Products*. Hoboken, N.J. : John Wiley & Sons, Inc.: Hoboken, N.J., 2012.

19. Adams, E. M.; Verreault, D.; Jayarathne, T.; Cochran, R. E.; Stone, E. A.; Allen, H. C., Surface Organization of a DPPC Monolayer on Concentrated SrCl2 and ZnCl2 Solutions. *Phys. Chem. Chem. Phys.* **2016,** *18* (47), 32345-32357.

20. Casper, C. B.; Verreault, D.; Adams, E. M.; Hua, W.; Allen, H. C., Surface Potential of DPPC Monolayers on Concentrated Aqueous Salt Solutions. *J. Phys. Chem. B* **2016,** *120* (8), 2043-52.

21. Adams, E. M.; Casper, C. B.; Allen, H. C., Effect of Cation Enrichment on Dipalmitoylphosphatidylcholine (DPPC) Monolayers at the Air-water Interface. *J. Colloid Interface Sci.* **2016,** *478* (C), 353-364.

22. Casillas-Ituarte, N. N.; Chen, X.; Castada, H.; Allen, H. C., Na(+) and Ca(2+) Effect on the Hydration and Orientation of the Phosphate Group of DPPC at Air-Water and Air-Hydrated Silica Interfaces. *J. Phys. Chem. B* **2010,** *114* (29), 9485-9495.

23. Lis, L. J.; Lis, W. T.; Parsegian, V. A.; Rand, R. P., Adsorption of divalent cations to a variety of phosphatidylcholine bilayers. *Biochemistry* **1981,** *20* (7), 1771-1777.

24. Schill, S. R.; Burrows, S. M.; Hasenecz, E. S.; Stone, E. A.; Bertram, T. H., The Impact of Divalent Cations on the Enrichment of Soluble Saccharides in Primary Sea Spray Aerosol. *Atmosphere* **2018,** *9* (12), 476-417.

25. Shultz, M. J.; Schnitzer, C.; Simonelli, D.; Baldelli, S., Sum Frequency Generation Spectroscopy of the Aqueous Interface: Ionic and Soluble Molecular Solutions. *Int Rev Phys Chem* **2000,** *19* (1), 123-153.
26. Ohno, P. E.; Wang, H. F.; Geiger, F. M., Second-order spectral lineshapes from charged interfaces. *Nat. Commun.* **2017,** *8* (1), 1032.
27. Ohno, P. E.; Wang, H. F.; Paesani, F.; Skinner, J. L.; Geiger, F. M., Second-Order Vibrational Lineshapes from the Air/Water Interface. *J. Phys. Chem. A* **2018,** *122* (18), 4457-4464.
28. Wen, Y.-C.; Zha, S.; Liu, X.; Yang, S.; Guo, P.; Shi, G.; Fang, H.; Shen, Y. R.; Tian, C., Unveiling Microscopic Structures of Charged Water Interfaces by Surface-Specific Vibrational Spectroscopy. *Physical Review Letters* **2016,** *116* (1), 016101.
29. Gonella, G.; Lütgebaucks, C.; de Beer, A. G. F.; Roke, S., Second Harmonic and Sum-Frequency Generation from Aqueous Interfaces Is Modulated by Interference. *The Journal of Physical Chemistry C* **2016,** *120* (17), 9165-9173.
30. Wen, Y.-C.; Zha, S.; Tian, C.; Shen, Y. R., Surface pH and Ion Affinity at the Alcohol-Monolayer/Water Interface Studied by Sum-Frequency Spectroscopy. *The Journal of Physical Chemistry C* **2016,** *120* (28), 15224-15229.
31. Doğangün, M.; Ohno, P. E.; Liang, D.; McGeachy, A. C.; Bé, A. G.; Dalchand, N.; Li, T.; Cui, Q.; Geiger, F. M., Hydrogen-Bond Networks near Supported Lipid Bilayers from Vibrational Sum Frequency Generation Experiments and Atomistic Simulations. **2018,** *122* (18), 4870-4879.
32. Reddy, S. K.; Thiraux, R.; Wellen Rudd, B. A.; Lin, L.; Adel, T.; Joutsuka, T.; Geiger, F. M.; Allen, H. C.; Morita, A.; Paesani, F., Bulk Contributions Modulate the Sum-Frequency Generation Spectra of Water on Model Sea-Spray Aerosols. *Chem* **2018,** *4* (7), 1629-1644.
33. Ohno, P. E.; Saslow, S. A.; Wang, H.-f.; Geiger, F. M.; Eisenthal, K. B., Phase-referenced nonlinear spectroscopy of the α-quartz/water interface. *Nature Communications* **2016,** *7*, 13587.
34. Ebben, C. J.; Ault, A. P.; Ruppel, M. J.; Ryder, O. S.; Bertram, T. H.; Grassian, V. H.; Prather, K. A.; Geiger, F. M., Size-Resolved Sea Spray Aerosol Particles Studied by Vibrational Sum Frequency Generation. *The Journal of Physical Chemistry A* **2013,** *117* (30), 6589-6601.
35. Velarde, L.; Zhang, X. Y.; Lu, Z.; Joly, A. G.; Wang, Z.; Wang, H. F., Communication: Spectroscopic Phase and Lineshapes in High-Resolution Broadband Sum Frequency Vibrational Spectroscopy: Resolving Interfacial Inhomogeneities of "Identical" Molecular Groups. *J. Chem. Phys.* **2011,** *135* (24), 241102.
36. Can, S. Z.; Mago, D. D.; Esenturk, O.; Walker, R. A., Balancing Hydrophobic and Hydrophilic Forces at the Water/Vapor Interface: Surface Structure of Soluble Alcohol Monolayers. *The Journal of Physical Chemistry C* **2007,** *111* (25), 8739-8748.
37. Esenturk, O.; Walker, R. A., Surface vibrational structure at alkane liquid/vapor interfaces. *J Chem Phys* **2006,** *125* (17), 174701.
38. Liu, W.; Fu, L.; Wang, Z.; Sohrabpour, Z.; Li, X.; Liu, Y.; Wang, H. F.; Yan, E. C. Y., Two Dimensional Crowding Effects on Protein Folding at Interfaces Observed by Chiral Vibrational Sum Frequency Generation Spectroscopy. *Phys. Chem. Chem. Phys.* **2018,** *20* (35), 22421-22426.
39. Lu, Z.; Karakoti, A.; Velarde, L.; Wang, W. N.; Yang, P.; Thevuthasan, S.; Wang, H. F., Dissociative Binding of Carboxylic Acid Ligand on Nanoceria Surface in Aqueous Solution: A Joint In Situ Spectroscopic Characterization and First-Principles Study. *J. Phys. Chem. C* **2013,** *117* (46), 24329-24338.

40. Mifflin, A. L.; Velarde, L.; Ho, J.; Psciuk, B. T.; Negre, C. F.; Ebben, C. J.; Upshur, M. A.; Lu, Z.; Strick, B. L.; Thomson, R. J.; Batista, V. S.; Wang, H. F.; Geiger, F. M., Accurate Line Shapes From sub-1 cm(-1) Resolution Sum Frequency Generation Vibrational Spectroscopy of Alpha-Pinene at Room Temperature. *J. Phys. Chem. A* **2015,** *119* (8), 1292-1302.
41. Olenick, L. L.; Chase, H. M.; Fu, L.; Zhang, Y.; McGeachy, A. C.; Dogangun, M.; Walter, S. R.; Wang, H. F.; Geiger, F. M., Single-Component Supported Lipid Bilayers Probed Using Broadband Nonlinear Optics. *Phys. Chem. Chem. Phys.* **2018,** *20* (5), 3063-3072.
42. Zhang, Z.; Guo, Y.; Lu, Z.; Velarde, L.; Wang, H. F., Resolving Two Closely Overlapping -CN Vibrations and Structure in the Langmuir Mono layer of the Long-Chain Nonadecanenitrile by Polarization Sum Frequency Generation Vibrational Spectroscopy. *J. Phys. Chem. C* **2012,** *116* (4), 2976-2987.
43. Blume, A., Lipids at the Air–Water Interface. *ChemTexts* **2018,** *4* (1), 1-25.
44. Gzyl-Malcher, B.; Paluch, M., Studies of Lipid Interactions in Mixed Langmuir Monolayers. *Thin Solid Films* **2008,** *516* (24), 8865-8872.
45. Gobrogge, C. A.; Kong, V. A.; Walker, R. A., Temperature-Dependent Partitioning of C152 in Binary Phosphatidylcholine Membranes and Mixed Phosphatidylcholine/Phosphatidylethanolamine Membranes. *J. Phys. Chem. B* **2017,** *121* (33), 7889-7898.
46. Kuo, R. R.; Chang, C. H.; Yang, Y. M.; Maa, J. R., Induced Removal of Dipalmitoyl Phosphatidylcholine by the Exclusion of Fibrinogen from Compressed Monolayers at Air/Liquid Interfaces. *J. Colloid Interface Sci.* **2003,** *257* (1), 108-115.
47. Amrein, M.; von Nahmen, A.; Sieber, M., A Scanning Force- and Fluorescence Light Microscopy Study of the Structure and Function of a Model Pulmonary Surfactant. *Eur. Biophys. J.* **1997,** *26* (5), 349-357.
48. Snyder, R. G.; Strauss, H. L.; Elliger, C. A., Carbon-Hydrogen Stretching Modes and the Structure of n-Alkyl Chains. 1. Long, Disordered Chains. *J. Phys. Chem.* **1982,** *86* (26), 5145-5150.
49. MacPhail, R. A.; Strauss, H. L.; Snyder, R. G.; Elliger, C. A., Carbon-Hydrogen Stretching Modes and the Structure of *n*-Alkyl Chains. 2. Long, All-Trans Chains. *J. Phys. Chem.* **1984,** *88* (3), 334-341.
50. Can, S. Z.; Mago, D. D.; Walker, R. A., Structure and Organization of Hexadecanol Isomers Adsorbed to the Air/Water Interface. In *Langmuir*, 2006; Vol. 22, pp 8043-8049.
51. Walker, R. A.; Gruetzmacher, J. A.; Richmond, G. L., Phosphatidylcholine Monolayer Structure at a Liquid−Liquid Interface. In *J. Am. Chem. Soc.*, 1998; Vol. 120, pp 6991-7003.
52. Conboy, J. C.; Messmer, M. C.; Richmond, G. L., Dependence of Alkyl Chain Conformation of Simple Ionic Surfactants on Head Group Functionality as Studied by Vibrational Sum-Frequency Spectroscopy. *J. Phys. Chem. B* **1997,** *101* (34), 6724-6733.
53. Fourkas, J. T.; Walker, R. A.; Can, S. Z.; Gershgoren, E., Effects of Reorientation in Vibrational Sum-Frequency Spectroscopy. *J. Phys. Chem. C* **2007,** *111* (25), 8902-8915.
54. Riske, K. A.; Barroso, R. P.; Vequi-Suplicy, C. C.; Germano, R.; Henriques, V. B.; Lamy, M. T., Lipid Bilayer Pre-Transition as the Beginning of the Melting Process. *Biochim. Biophys. Acta* **2009,** *1788* (5), 954-963.
55. Kodama, M.; Kuwabara, M.; Seki, S., Sucessive Phase-transition Phenomena and Phase Diagram of the Phosphatidylcholine-Water System as Revealed by Differential Scanning Calorimetry. *Biochim. Biophys. Acta, Biomembr.* **2002,** (689), 567-570.

56. McElhaney, R. N., The Use of Differential Scanning Calorimetry and Differential Thermal-Analysis in Studies of Model and Biological-Membranes. *Chem Phys Lipids* **1982,** *30* (2-3), 229-259.
57. Jain, M. K.; Wu, N. M., Effect of Small Molecules on the Dipalmitoyl Lecithin Liposomal Bilayer: III. Phase Transition in Lipid Bilayer. *J. Membr. Biol.* **1977,** *34* (1), 157-201.

TOC Figure